

# Vortex Nucleation in a Stirred Bose-Einstein Condensate

C. Raman, J. R. Abo-Shaeer, J. M. Vogels, K. Xu, and W. Ketterle

*Department of Physics, MIT-Harvard Center for Ultracold Atoms, and Research Laboratory of Electronics, MIT, Cambridge, MA 02139*

(November 3, 2018)

We studied the nucleation of vortices in a Bose-Einstein condensate stirred by a laser beam. We observed the vortex cores using time-of-flight absorption imaging. By varying the size of the stirrer, we observed either discrete resonances or a broad response as a function of the frequency of the stirrer's motion. Stirring beams small compared to the condensate size generated vortices below the critical rotation frequency for the nucleation of surface modes, suggesting a local mechanism of generation. In addition, we observed the centrifugal distortion of the condensate due to the rotating vortex lattice and found evidence for bent vortices.

PACS 03.75.Fi, 67.40.Vs, 32.80.Pj

Dissipation and turbulence in superfluid flow often involves the creation and subsequent motion of quantized vortices [1]. Since vortices are topological defects they may only be created in pairs, or can enter a system individually from its boundary. The nucleation process has been a subject of much theoretical interest [2]. Experiments with Bose-Einstein condensates (BEC) confined in atom traps are well suited to test theories of nucleation because the boundary of the condensate is well controlled, and vortices can be directly imaged.

Vortex nucleation usually involves dynamical instabilities and superfluid turbulence [1,2]. Exceptions are the direct coupling between ground and vortex states for small condensates [3] and the engineering of states of quantized circulation by manipulating the phase of the wavefunction [4–6]. Turbulent flow can be created by perturbing the system with a time-dependent boundary, for example by a small laser beam [7,8], or by a rotating trap anisotropy [9–11]. The resulting vortices have been directly imaged [8–10].

In a rotating frame, vortices are energetically favored above a critical rotational frequency  $\Omega_c$  [2,12]. Current theories suggest that the nucleation of vortices requires the creation of surface waves which “collapse” into a vortex state [13–17]. This corresponds to the disappearance of the energy barrier for a vortex to enter the cloud [2,14,18]. For surface excitations with angular momentum  $l\hbar$  and frequency  $\omega_l$ , the minimum rotational frequency is

$$\Omega_s = \min_l(\omega_l/l). \quad (1)$$

This corresponds to a Landau critical velocity for surface waves  $v_c = \Omega_s R_{\text{TF}}$ , where  $R_{\text{TF}}$  is the Thomas-Fermi radius [15].

Our main result is that vortices can be created *below*  $\Omega_s$  by using a small, localized stirring beam. This indicates that the current surface mode analysis of vortex nucleation is incomplete. Recent experiments [9,19] observed vortices only at much *higher* frequencies, giving rise to a variety of theoretical models [17,20]. One explanation is that those experiments excited only the  $l = 2$

mode, which requires a higher drive frequency than Eqn. (1) [19,21,22]. We verified this prediction by stirring the condensate with anisotropies of different symmetries ( $l = 2, 3, 4$ ) and observing distinct resonance frequencies for vortex formation. If the condensate is stirred with a small beam, one would expect to couple to many modes  $l$ . Surprisingly, the small stirrer did not excite resonances, but could nonetheless generate vortices as effectively as a resonant drive.

Our method of vortex generation has been outlined in previous work [10]. We start with nearly pure BECs ( $> 90\%$  condensate fraction) of up to  $5 \times 10^7$  sodium atoms in a cylindrically shaped Ioffe-Pritchard magnetic trap with radial and axial frequencies of  $\omega_r = 2\pi \times 83$  Hz and  $\omega_z = 2\pi \times 20$  Hz, respectively. A radio frequency “shield” limited the magnetic trap depth to 50 kHz (2.3  $\mu\text{K}$ ). The condensate chemical potential and peak density were 300 nK and  $4 \times 10^{14}$   $\text{cm}^{-3}$ , respectively, corresponding to a healing length  $\xi \simeq 0.2$   $\mu\text{m}$ .

Vortices were generated by rotating the condensate along its long axis with a scanning blue-detuned laser beam (532 nm) [23]. We explored different beam waists between 5 and 25  $\mu\text{m}$ . For the tightest focus, the peak optical dipole potential was 620 nK. We used scan radii as large as the Thomas-Fermi radius  $R_{\text{TF}}$ , which varied from 27–30  $\mu\text{m}$ . Multiple beam patterns (formed by rapidly scanning the laser beam from 1.5–10 kHz) were used to create vortices. The laser beam was left on during evaporation to damp out dipole motion of the condensate. Immediately after producing a condensate we began the rotation for times of up to 500 ms, generating a vortex tangle. The laser beams were then instantly shut off and the cloud equilibrated for 500 ms, during which time the vortices crystallized into an Abrikosov lattice as shown in Fig. 4c and detailed in previous work [10]. For small numbers of vortices the gas did not fully settle into a regular lattice before imaging.

The vortex cores were observed using resonant absorption imaging after 41 ms of ballistic expansion, which magnified them by 20 from their size  $\xi$  in the trap. As in

our previous work we imaged a 50-150  $\mu\text{m}$  slice of atoms in the center of the cloud using spatially selective optical pumping into the  $F = 2$  to  $F = 3$  cycling transition [10].

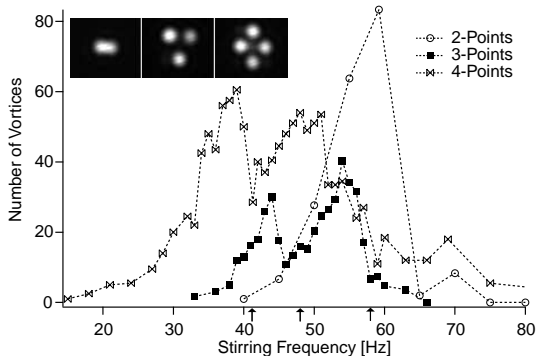


FIG. 1. Discrete resonances in vortex nucleation. The number of vortices created by multi-point patterns is shown. The condensate radius was  $R_{\text{TF}} = 28 \mu\text{m}$ . Each data point is the average of three measurements. The arrows below the graph show the positions of the surface mode resonances  $\omega_l = \omega_r/\sqrt{l}$ . The stirring times were 100 ms for the 2- and 3-point data, and 300 ms for the 4-point data. Inset shows 2-, 3-, and 4-point dipole potentials produced by a 25  $\mu\text{m}$  waist laser beam imaged onto the CCD camera. The separation of the beams from the center is 25  $\mu\text{m}$  for the 2-point pattern and 55  $\mu\text{m}$  for the 3- and 4-point patterns. The laser power per spot was 0.35 mW, 0.18 mW, and 0.15 mW for the 2-, 3- and 4-point data, respectively.

By varying the stirring parameters we explored different mechanisms for vortex nucleation. A large stirrer, with a beam waist comparable to the Thomas-Fermi radius showed enhanced vortex generation at discrete frequencies. Fig. 1 shows the number of vortices versus the frequency of rotation of the laser beam using 2-, 3- and 4-point patterns. The total laser beam power corresponded to an optical dipole potential between 60 nK and 240 nK. The resonances were close to the frequencies of excitation of  $l = 2, 3$  and 4 surface modes ( $\omega_l = \omega_r/\sqrt{l}$ ) [13]. A second, higher resonance appeared in the 3- and 4-point data, presumably due to additional coupling to the quadrupole ( $l = 2$ ) mode. The shift in the position of the peaks from the frequencies  $\omega_l$  of elementary excitations is probably due to the presence of the stirrer and the vortices.

Our results clearly show discrete resonances in the nucleation rate of vortices which depend on the geometry of the rotating perturbation. This confirms the role of discrete surface modes in vortex formation. A dependence on the symmetry of the stirrer (1-point versus 2-point) has also been explored in Paris [22]. For longer stirring times and higher laser powers the condensate accommodated more vortices at all frequencies, and the resonances became less pronounced.

A stirrer much smaller than the condensate size could generate vortices very rapidly – more than 100 vortices

were created in 100 ms of rotation. Fig. 2a shows the number of vortices produced using a 2-point pattern with a scan radius close to  $R_{\text{TF}}$  for various stirring times. Above 300 ms the angular momentum of the cloud appeared to saturate and even decreased, accompanied by visible heating of the cloud.

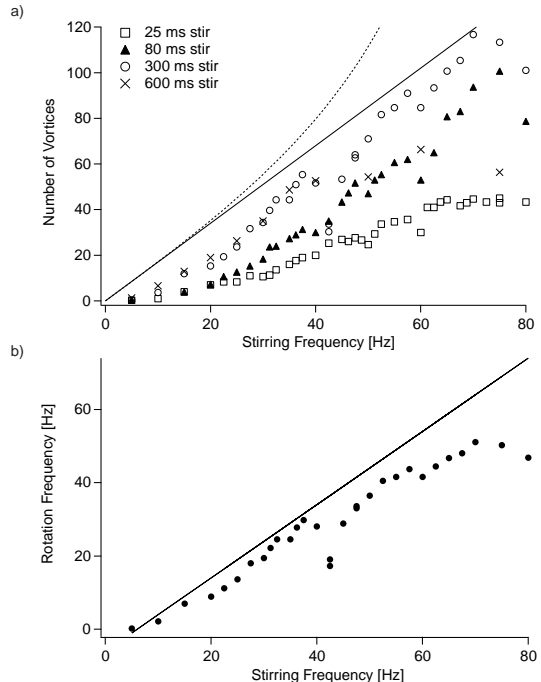


FIG. 2. Nonresonant nucleation using a small stirrer. (a) Average number of vortices created for different stirring times using a 2-point pattern positioned at the edge of the condensate. The beam waist, total power, and separation are 5.3  $\mu\text{m}$ , 0.16 mW, and 54  $\mu\text{m}$ , respectively. (b) Effective lattice rotation frequency as a function of stir frequency. The lines in both graphs indicate the predictions of different models described in the text.

The maximum number of vortices was roughly proportional to the stirring frequency. For a lattice rotating at frequency  $\Omega$ , the quantized vortex lines are distributed with a uniform area density  $n_v = \frac{2\Omega}{\kappa}$ , where  $\kappa = h/M$  is the quantum of circulation and  $M$  the atomic mass [12]. Therefore, the number of vortices at a given rotation frequency should be

$$N_v = 2\pi R^2 \Omega / \kappa \quad (2)$$

in a condensate of radius  $R$ . The straight line in Fig. 2a assumes  $R = R_{\text{TF}}$  and that the lattice has equilibrated with the drive. In contrast to the large stirrer no resonances were visible even when the number of vortices had not yet saturated. This suggests a different mechanism for vortex nucleation. Further evidence for this was obtained from the frequency and spatial dependences.

For our experimental conditions, Eqn. 1) yields  $\Omega_s \simeq 0.25\omega_r = 21 \text{ Hz}$  [24]. With the small stirrer, we observed vortices at frequencies as low as 7 Hz. Below

this frequency the velocity of the stirrer was not much larger than the residual dipole oscillation of the condensate. The rotational frequency below which a rectilinear vortex in the condensate center is energetically favored is 7 Hz [2].

In Fig. 3 we varied the radius of the 2-point scan. The frequency of rotation was chosen to keep the linear velocity of the laser beam constant. Vortices could be generated over a broad range of radii. The maximum number was obtained at intermediate radii rather than the Thomas-Fermi surface, providing further evidence that surface excitations of the unperturbed condensate are not the dominant nucleation mechanism. The observed radial dependence makes it unlikely that the thermal cloud plays a crucial role in the vortex nucleation, since at very low temperatures its maximum density occurs at the surface of the condensate. Indeed, we observed that finite temperatures increased the damping and led to fewer vortices.

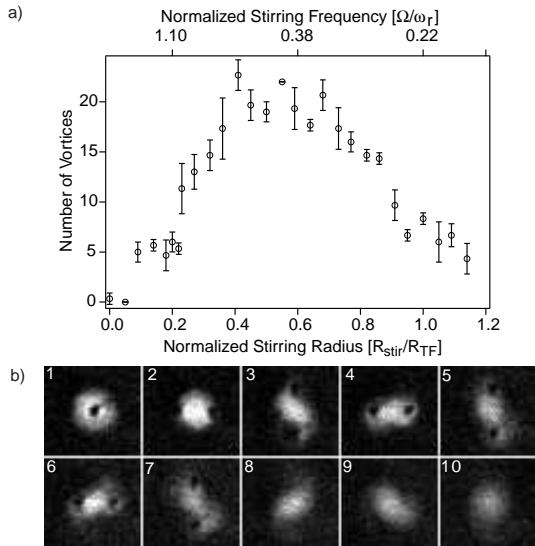


FIG. 3. Spatial dependence of vortex nucleation. (a) Shown is the number of vortices as a function of the stirring radius for a constant stirring velocity (0.2  $c$ ). At the Thomas-Fermi radius, the angular frequency of the stirrer was 17.5 Hz. The error bars reflect the scatter of 3 measurements at the same radius. (b) Axial phase contrast images showing the pure condensate with the aligned stirrer (1), the condensate during (2-7) and after (8-10) stirring.

The nucleation mechanism for small stirrers may be related to our earlier experiments on the onset of dissipation in stirred condensates, where we observed a drag force at velocities above  $\sim 0.1c$ , where  $c$  is the speed of sound at the condensate center [7,25]. The friction with the moving stirrer causes an asymmetry in the density profile in front of and behind the laser beam. This has been directly imaged for linear motion [25]. Similar flow field effects can be observed in Fig. 3b, where they are clearly linked to the formation of vortices. Vortex pairs

are predicted to arise from linear stirring [26,27]. When the laser beam moves in a circle, co-rotating vortices will be favored, whereas counter-rotating vortices will be expelled from the system.

For an object smaller than the healing length  $\xi$ , the critical velocity for vortex formation occurs at the Landau value given by Eqn. (1). For objects larger than  $\xi$  such as our laser beam, hydrodynamic flow around the stirrer can reduce the critical velocity relative to Eqn. (1) [26], which may explain our observation of vortices below 21 Hz.

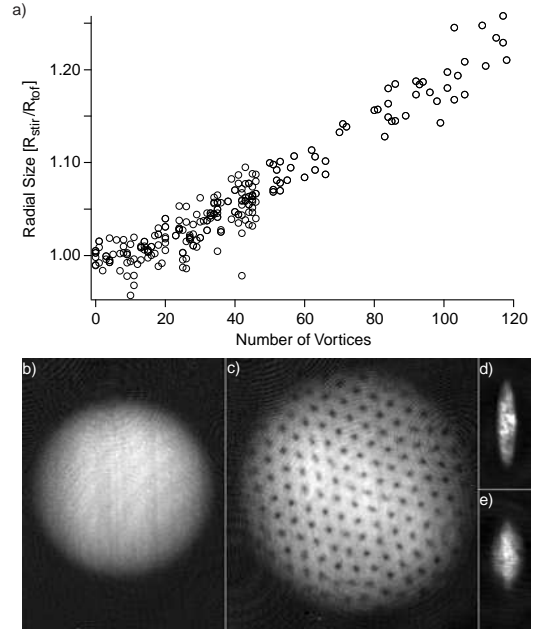


FIG. 4. Centrifugal effects on a rotating condensate. Shown is the observed radial size of the condensate versus vortex number. The condensate size was determined from a parabolic fit to the time-of-flight distribution after 41.5 ms. (b,c) Comparison of a non-rotating condensate ( $R_{\text{tof}} = 570 \mu\text{m}$ ) and one with 160 vortices. Radial in-situ phase contrast imaging of a condensate at rest (d) and in rotation at a frequency of 75 Hz (e), showing the modified aspect ratio. The length of the condensate in (d) was  $200 \mu\text{m}$ .

In our earlier work we observed that the size of a condensate with vortices exceeded the size of the non-rotating condensate [10]. Here we study these centrifugal distortions quantitatively (also note [11]). Fig. 4 shows the enhancement of the cloud size  $R$  in time-of-flight by up to 25% due to additional rotational kinetic energy. The rotating condensate experiences a centrifugal potential  $-(1/2)M(\Omega r)^2$ , which leads to an effective radial trapping frequency of  $\sqrt{\omega_r^2 - \Omega^2}$ . For a constant number of atoms  $N$ , this increases the Thomas Fermi radius

$$R_{\text{TF}} = \frac{R_0}{(1 - (\frac{\Omega}{\omega_r})^2)^{3/10}} \quad (3)$$

and reduces the mean-field interaction energy  $E_{\text{int}}$ . The

total release energy of the gas is then  $E = E_{int} + \frac{1}{2}I_{\text{eff}}\Omega^2 + E_{v0}N_v$ . The 2nd term accounts for the rigid rotation of the lattice while the 3rd term is a quantum correction due to the kinetic energy of the cores, and is negligible for large  $N_v$ . The effective moment of inertia of the condensate is  $I_{\text{eff}} = 2/7MR_{\text{TF}}^2N$ . The energy per unit length of a single vortex is  $E_{v0} = \pi n\hbar^2/M \ln[0.27d/\xi]$ , where  $d = n_v^{-1/2}$  is the mean distance between vortices [28]. When we average  $E_{v0}$  over the Thomas-Fermi distribution we predict a 30% increase in  $E$  for 120 vortices, whereas the observed increase in  $R^2$  is about 50%. This discrepancy is probably due to our selection of the central slice of the cigar, where the rotational energy is the highest, and due to the unobserved axial expansion, which may depend on the angular momentum of the cloud.

If we account for centrifugal effects and combine Eqns. (2) and (3), we expect a divergence of the number of vortices near the trap frequency (dashed line in Fig. 2a). The deviation of the data from this line suggests that the condensate did not fully equilibrate with the rotating drive. Taking into account the critical velocity for vortex nucleation,  $v_c \simeq 0.1c$  [25], we expect the maximum rotation frequency of the lattice to be  $\Omega_S - v_c/R_{\text{TF}}$  where  $\Omega_S$  is the frequency of the stirrer moving at radius  $R_{\text{TF}}$ . Using the measured number of vortices, we can invert Eqns. (2) and (3) to derive the lattice rotation frequency, which is shown in Fig. 2b, along with the expected value  $\Omega_S - 2\pi \times 6$  Hz assuming a constant  $N$ . The discrepancy can be partly attributed to loss of atom number due to heating by the stirrer, which was up to 30%. We can also derive from these equations the flow velocity at the edge of the condensate. For a lattice with 144 vortices, this velocity exceeded the speed of sound at the condensate center by 40%, in contrast to a recent suggestion that supersonic rotation speeds are unattainable [33].

At low rotational velocities, vortices should not be recilinear as assumed in many theoretical calculations but bent [29,30]. Such bent vortices should have lower visibility in our images due to the line of sight integration across the optically pumped condensate slice. Fig. 5 shows several examples. Some appear as vortex lattices with tilted vortex cores. Other images show structures reminiscent of half rings and coiled vortices. However, since these are time-of-flight images it is not obvious how some of the observed features are related to spatial structures in the trapped condensate.

In conclusion, we have studied the nucleation of vortices in condensates stirred by rotating laser beams and identified two different nucleation mechanisms, surface modes for large stirrers, as well as local turbulence for small stirrers. So far, we have mainly concentrated on pure condensates, but it will be intriguing to study the vortex phase diagram at finite temperatures [31,32] and the role of the thermal cloud in the decay of vortices [33].

We thank J.R. Anglin, D. Feder, A. E. Leanhardt and A.P. Chikkatur for useful discussions. This research is supported by NSF, ONR, ARO, NASA, and the David and Lucile Packard Foundation.

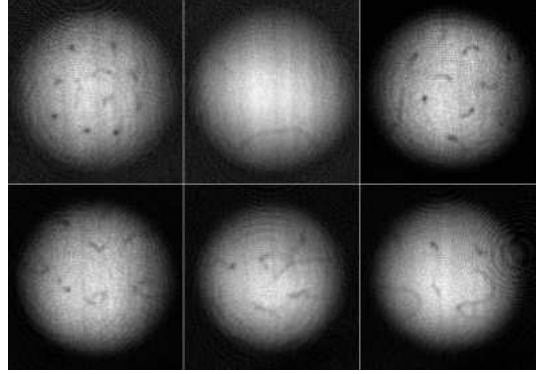


FIG. 5. Three-dimensional structure of vortices. Shown are several examples of time-of-flight pictures of condensates at low rotational frequencies, where "smeared-out" vortex cores and elongated features were observed. The radius of the condensate was  $510 \mu\text{m}$ .

- 
- [1] R. J. Donnelly, *Quantized vortices in helium II* (Cambridge University Press, Cambridge, 1991).
  - [2] A. L. Fetter and A. A. Svidzinsky, *J. Phys.: Condens. Matter* **13**, R135R194 (2001).
  - [3] B. M. Caradoc-Davies, R. J. Ballagh, and K. Burnett, *Phys. Rev. Lett.* **83**, 895 (1999).
  - [4] M. R. Matthews *et al.*, *Phys. Rev. Lett.* **83**, 2498 (1999).
  - [5] Dobrek *et al.*, *Phys. Rev. A* **60**, R3381 (1999).
  - [6] K.-P. Marzlin and W. Zhang, *Phys. Rev. A* **57**, 4761 (1998).
  - [7] C. Raman *et al.*, *Phys. Rev. Lett.* **83**, 2502 (1999).
  - [8] S. Inouye *et al.*, preprint cond-mat/0104444.
  - [9] K. W. Madison, F. Chevy, W. Wohlleben, and J. Dalibard, *Phys. Rev. Lett.* **84**, 806 (2000).
  - [10] J. R. Abo-Shaer, C. Raman, J. M. Vogels, and W. Ketterle, *Science* **292**, 476 (2001).
  - [11] P. Haljan, talk at DAMOP, London, Ontario, May 2001.
  - [12] P. Nozières and D. Pines, *The Theory of Quantum Liquids* (Addison-Wesley, Redwood City, CA, 1990).
  - [13] F. Dalfovo *et al.*, *Phys. Rev. A* **56**, 3840 (1997).
  - [14] T. Isoshima and K. Machida, *Phys. Rev. A* **60**, 1313 (1999).
  - [15] U. A. Khawaja, C. J. Pethick, and H. Smith, *Phys. Rev. A* **60**, 1507 (1999).
  - [16] F. Dalfovo and S. Stringari, *Phys. Rev. A* **63**, 011601 (2001), M. Tsubota, K. Kasamatsu, and M. Ueda, preprint cond-mat/0104523.
  - [17] D. L. Feder, A. A. Svidzinsky, A. L. Fetter, and C. W. Clark, *Phys. Rev. Lett.* **86**, 564 (2001).
  - [18] D. L. Feder, C. W. Clark, and B. I. Schneider, *Phys. Rev. A* **61**, 011601(R) (1999).
  - [19] K. W. Madison, F. Chevy, V. Bretin, and J. Dalibard, *Phys. Rev. Lett.* **86**, 4443 (2001).
  - [20] J. J. García-Ripoll and V. M. Pérez-García, preprint cond-mat/0006368.
  - [21] S. Sinha and Y. Castin, preprint cond-mat/0101292 18.

- [22] F. Chevy, K. W. Madison, V. Bretin, and J. Dalibard, preprint cond-mat/0104218.
- [23] R. Onofrio *et al.*, Phys. Rev. Lett. **84**, 810 (2000).
- [24] D. Feder, private communication.
- [25] R. Onofrio *et al.*, Phys. Rev. Lett. **85**, 2228 (2000).
- [26] T. Frisch, Y. Pomeau, and S. Rica, Phys. Rev. Lett. **69**, 1644 (1992).
- [27] B. Jackson, J. F. McCann, and C. S. Adams, Phys. Rev. Lett. **80**, 3903 (1998).
- [28] D. Stauffer and A. Fetter, Phys. Rev. **168**, 156 (1968).
- [29] J. J. García-Ripoll and V. M. Pérez-García, preprint cond-mat/01021297.
- [30] A. Aftalion and T. Riviere, preprint cond-mat/0105208.
- [31] S. Stringari, Phys. Rev. Lett. **82**, 4371 (1999).
- [32] T. Mizushima, T. Isoshima, and K. Machida, preprint cond-mat/0104358.
- [33] P. O. Fedichev and A. E. Muryshev, preprint, cond-mat/0004264.